Formation of fingerlike structures in fragmentation of small-scale patchy aurora

Yasutaka Hiraki[1] and Kaori Sakaguchi[2]

Received 30 April 2010; revised 30 August 2010; accepted 7 September 2010; published 29 December 2010.

[1] Recent high-resolution video imagery reveals a dynamic feature of small-scale (< 20 km) patchy aurora during a substorm recovery phase, that is, fingerlike structures with a few kilometers' scale are formed through the patch fragmentation. Various kinetic processes such as ion finite Larmor radius effects can be involved because the scale mapped into the plasma sheet is much smaller than the ion inertia length. However, such a scale is likely to be strongly damped in a high-β plasma regime by the ion gyroviscosity effect. In this study, we make several 2.5-dimensional simulations at the system of each position s along a field line, perpendicular to the ambient magnetic field, by means of the three-field reduced magnetohydrodynamic equations. The model includes the effects of ion diamagnetic drift and electron parallel motion. In a low-β regime of $s = 4\ R_E$, we find that an ion diamagnetic drift wave grows isotropically to form a patchy structure with a scale of ≈10 km. As the field-aligned current increases, these patches are fragmented and fingerlike structures with scales of 2–5 km appear owing to the nonlinear electron inertia effect. The scales of patches and fingers and the east–westward finger development, as well as the time scale, are fairly consistent with those of recent observations. On the other hand, at the plasma sheet (ion beta $\beta_i = 1$, $s = 7.5\ R_E$), fingerlike patterns cannot be formed owing to a predominance of large-scale vortex patterns.

Citation: Hiraki, Y., and K. Sakaguchi (2010), Formation of fingerlike structures in fragmentation of small-scale patchy aurora, *J. Geophys. Res.*, *115*, A12253, doi:10.1029/2010JA015623.

1. Introduction

[2] The patchy aurora exhibits an inhomogeneous bright structure in the diffuse aurora throughout latitudes of the main auroral oval. It often appears at the postmidnight sector in magnetic local time during the substorm recovery phase [*Akasofu*, 1974]. The spatial scale varies from 10 km to >200 km, and it is mostly accompanied by pulsations with a period of 0.3–30 s [*Davis*, 1978]. Large-scale wavelike undulations (>200 km) observed mainly in the premidnight sector at the lower latitude have been well investigated by DMSP, TIMED, and IMAGE satellites [*Lui et al.*, 1982; *Zhang et al.*, 2005; *Goldstein et al.*, 2005] and by ground-based all-sky cameras [e.g., *Nishitani et al.*, 1994]. These are explained by the Kelvin-Helmholtz instability owing to a large-scale sheared convection in the inner magnetosphere [e.g., *Yamamoto et al.*, 1993].

[3] Recent high-resolution camera observations capture the dynamics of small-scale patch auroras (≤20 km) [*Shiokawa et al.*, 2010]. It is found that fingerlike shapes with a scale of a few kilometers are produced in the vicinity of the patch auroras, and new small structures are formed through its fragmentation within a few minutes. It is also found that the background auroral luminosity reveals a pulsation with a period of tens of seconds. They presented that this fingerlike structure is formed by the Rayleigh-Taylor instability due to a high β gradient at the plasma sheet and is associated with the retainment of patch auroras. Furthermore, the direction of the finger development is found to be east–westward, which implies an azimuthal force balance between magnetic and pressure fields at the plasma sheet. The condition seems to be unusual as a large-scale pressure gradient as well as magnetic curvature can be formed mainly in the radial direction, and thus further mechanisms need to be supplemented.

[4] A different type of structures with a scale ≈1.8 km is captured by recent Reimei satellite observations at the equatorward edge of the diffuse aurora in a magnetically quiet condition [*Ebihara et al.*, 2010]; it is also located in the postmidnight sector. The snapshots are likely to be characterized by small-scale patches (≈10 km) and fingers (≈1.8 km) that are similar to the structures obtained by *Shiokawa et al.* [2010]. They presented data indicating that trigger mechanisms of the "smokelike" structures are pitch angle scattering of hot electrons (≥1 keV) by whistler modes and some cold plasma instabilities. The energy-time spectrogram and simultaneous satellite data reveal increases in the hot electron flux and pressure during the event, whereas the spectrum in colder electrons is somewhat featureless. As they pointed out, a high-pressure regime can be formed in the inner magnetosphere through a hot electron injection, and then various waves and instabilities are excited.

[1]National Institute for Fusion Science, Toki, Japan.
[2]National Institute of Information and Communications Technology, Tokyo, Japan.

0148-0227/10/2010JA015623

[5] Numerical studies of similar structures driven by the interchange instability, or the Rayleigh-Taylor instability, were performed by magnetohydrodynamic (MHD) and hybrid plasma simulations including ion finite Larmor radius (FLR) effects in a moderate-β regime as $\approx$0.1 [*Huba and Winske*, 1998; *Lewis et al.*, 2005]. They reproduce a fingerlike feature in the ion pressure as well as its variation due to the nonlinear effects. However, it seems to be natural to consider that the small-scale patch aurora we focus on here, located out of closed field lines, is a manifestation of the field-aligned current rather than the plasma pressure. The fact is also supported by the east–westward development of fingers; the finger seems to develop north–southward if it reflects a pressure pattern.

[6] On the other side, many studies of small-scale auroral arc dynamics ($\leq$10 km), such as splitting of arcs, were vigorously performed in association with the kinetic Alfvén wave [*Rankin et al.*, 1999; *Chaston et al.*, 2006; 2008; *Lysak and Song*, 2008]. In this case, the electron inertia effect in a low-β condition around the acceleration region, or a position along the field line s = 1–2 R_E (Earth radius), has a dominant role in the formation of strong parallel electric field, leading to auroral brightening by accelerated electrons.

[7] The purpose of this study is to reproduce the fingerlike structures during fragmentation of the patch structures reported by *Shiokawa et al.* [2010]. We perform a 2.5-dimensional reduced MHD model simulation including ion and electron inertia effects and demonstrate that these structures are formed spontaneously in the field-aligned current from a featureless initial condition. Here, we assume the conditions of various positions, s = 1–7.5 R_E, for the modeled magnetic flux tube of $L \approx 6.9$ at the observation site; the magnetic curvature is also estimated to be $\approx$7 R_E with the Tsyganenko-96 model. One may suppose that these small structures (patches and fingers) are driven by a cascade due to the ion inertia and FLR effects at the plasma sheet. However, scales less than the ion inertia length seem to be strongly damped by the FLR effect or gyroviscosity in high-β plasmas. Thus, we also investigate whether it is possible to reproduce these small structures in the plasma sheet condition. An implication of the smokelike structures in *Ebihara et al.* [2010] is provided in section 4.

2. Model Description

[8] The four-field model is an extension of reduced-MHD description based on the flute ordering $k_\parallel/k_\perp = \mathcal{O}(\epsilon)$ and thus appropriate to treat nonlinear plasma dynamics in the magnetosphere-ionosphere (MI) coupling region [*Hazeltine et al.*, 1987; *Stasiewicz et al.*, 2000]; $k_\parallel$ and $k_\perp$ are parallel and perpendicular wave numbers to the ambient magnetic field B_0, and ϵ is a small number. It easily includes ion FLR effects, diamagnetic drift waves, and the effects of long mean free path electron adiabatic motions. These processes are considered to be critical in discussing auroral fine scales of our interest, especially in the low-β region as $\beta \leq 10^{-2}$ (a position of $s \approx$ 1–6 R_E). It is noted, however, that this model is valid only for thermal ions with short mean free path parallel motion and does not treat wave-particle interactions such as the Landau damping. In this study, we omit the compressional terms and hence the equation for parallel ion velocity for simplicity because the small-scale structures of interest would be formed in a low-temperature regime. Thus, the model is further reduced to be a three-field system. Including terms owing to finite electron inertia in the parallel Ohm's law [*Aydemir*, 1992], the three-field equations for a generalized vorticity ζ, parallel vector potential ψ, and electron pressure p can be written as follows:

$$\partial_t \zeta + \{F, \zeta\} = -\nabla_\parallel j_\parallel - (1+\tau)\kappa \partial_y p + \nu \nabla_\perp^2 \zeta + \delta\tau \nabla_\perp \cdot \{p, \nabla_\perp F\} \tag{1}$$

$$\partial_t \psi + \nabla_\parallel (\phi - \delta p) = \eta j_\parallel + \delta_e \left(\partial_t j_\parallel + \{\phi - \delta p, j_\parallel\}\right) \tag{2}$$

$$\partial_t p + \{\phi - \delta p, p\} = -\beta' \partial_y (\phi - \delta p) + D \nabla_\perp^2 p. \tag{3}$$

Equation (1) is derived from the ion equation of motion and includes kink and line-bending effects as the right-hand first term and interchange effect as the second term. Here the field-aligned current is provided as $j_\parallel = \nabla_\perp^2 \psi$. As the FLR correction, we take the Braginskii's tensor for ion gyroviscosity effect shown in the last term in equation (1) [*Braginskii*, 1965]. A generalized potential $F = \phi + \delta\tau p$ means a stream function in the sense that the ion velocity transverse to B_0 is $v_\perp = b_0 \times \nabla_\perp F$, yielding the combination of electric and diamagnetic drifts; ϕ is the electric potential, τp the ion pressure, and the meanings of δ and τ are shown just below. It is equivalent to consider the Hall effect due to the current $j_\perp \sim b_0 \times \nabla_\perp \delta\tau p + \mathcal{O}(\epsilon)$ where the inertia current is included in the first-order term. The ion vorticity is written as $\zeta = b_0 \cdot \nabla_\perp \times v_\perp = \nabla_\perp^2 F$. On the other hand, the electron diamagnetic drift is included as $-\delta p$ in equations (2) and (3). In equation (3), we consider the effect of a large-scale pressure gradient β' perpendicular to B_0 as the right-hand first term.

[9] Spatial ($\nabla_\perp$, $\nabla_\parallel$) and time (∂_t) derivatives are normalized by the characteristic scales $L_\perp$ and $t_s = L_\perp/v_A$, where v_A is the Alfvén velocity. We use the Poisson bracket symbol as $\{f,g\} = b_0 \cdot \nabla_\perp f \times \nabla_\perp g$, and the parallel gradient operator is defined by $\nabla_\parallel f = \nabla_s f + \{f, \psi\}$; b_0 is a unit vector along a field line s and ∇_s is a derivative to the direction. Three field variables, ϕ, ψ, and p, are also normalized by $\phi_s = v_A B_0 L_\perp/c$, $\psi_s = B_0 L_\perp$, and $p_s = B_0^2/8\pi$, respectively. In addition to the above normalized variables, the model involves five constant parameters: the electron beta $\beta = n_e k T_e/p_s$, the temperature ratio $\tau = T_i/T_e$, the ion FLR parameter $\delta = \lambda_i/2L_\perp$, the finite electron inertia parameter $\delta_e = \lambda_e^2/L_\perp^2$, and the magnetic curvature $\kappa = b_0 \cdot \nabla b_0$ with $\lambda_{i,e}$ being the ion and electron inertia lengths. The viscosity and the resistivity coefficients are set to be small as $\nu = \eta = D = 10^{-6}$.

[10] We describe our model geometry as well as the detail of β'. We treat the system where the perpendicular scale $L_\perp$, standing for auroral fine structures, is much smaller than the parallel scale $L_\parallel$, or the wavelength of the shear Alfvén wave. We assume that a standing wave exists along a field line and reduce this model to the 2.5-dimensional system. Thus, the operator $\nabla_\parallel$ seen in the equations is written as $\nabla_\parallel = \alpha - \{\psi,\}$, where $\alpha = L_\perp/L_\parallel$ represents the wave number of a standing wave normalized by $L_\perp^{-1}$. By this simplification, we do not treat the effects of nonlinear dynamics of the shear Alfvén wave and the MI coupling. Our coordinate system is equivalent to the geocentric coordinate, where x and y are latitudinal and longitudinal distances, respectively. The spa-

Table 1. The Background Conditions of the System at Each Field-Line Position s[a]

s	2 R_E	4 R_E	6 R_E	7.5 R_E
B_0 [G]	2.60 (−2)	4.90 (−3)	1.70 (−3)	7.60 (−4)
n_e [cm^{-3}]	6.54	1.70	1.14	1.03
T_e [eV]	1.49	43.4	547	1390
v_A [cm/s]	2.21 (9)	8.19 (8)	3.47 (8)	1.63 (8)
t_s [s]	9.33 (−3)	4.96 (−2)	1.43 (−1)	3.20 (−1)
$L_\perp$ [km]	207	407	497	523
β	5.80(−7)	1.24 (−4)	9.14 (−3)	0.100
ϕ_s [V]	1.19 (4)	1.63 (3)	292	64.7
ψ_s [G cm]	5.38 (5)	1.99 (5)	8.43 (4)	3.96 (4)
$j_{\parallel s}$ [μA/m^2]	9.99	0.958	0.272	0.115
λ_i [km]	89.0	174	213	224
λ_e [km]	2.07	4.07	4.97	5.23

[a]Magnetic field B_0 is estimated from the Tsyganenko-96 model, for a magnetic flux tube of $L \approx 6.9$ corresponding to the observation site of our interest. Plasma density n_e is taken from *Streltsov and Lotko* [2003]. A similar profile is used for electron temperature T_e, but the ion beta is assumed to approach unity at the plasma sheet (s = 7.5 R_E in our case) where the electron beta β is 0.1. v_A is the Alfvén velocity, t_s, $L_\perp$, ϕ_s, ψ_s, and $j_{\parallel s}$ are the characteristic time, perpendicular scale, electric potential, vector potential, and field-aligned current, respectively; λ_i and λ_e are the ion and electron inertia lengths. Numbers in parentheses (m) mean $\times 10^m$. Note that for usage units of field-aligned current and spatial scale are set to be μA/m^2 and km, respectively, while s is normalized by earth radius R_E.

tial scales vary with a field-line position s according to the flux tube expansion. On the plasma sheet, x points tailward and y points eastward. We put an Earthward pressure gradient by defining $\beta' = -\partial_{x0}\beta = \beta L_\perp / L_c$; it is related to the growth of interchange modes. Here we suppose that a high-β regime is formed locally in the plasma sheet ($\beta' > 0$), and the scale of the gradient is equal to that of the magnetic curvature L_c; *Lewis et al.* [2005] imposed a similar assumption.

[11] To obtain the constant parameters in equations (1)–(3), we provide the characteristic values of electron density n_s, temperature T_e, magnetic field B_0, several spatial scales $L_\perp$, $L_\parallel$, and L_c at each position s. We show the plasma parameters as well as the constants in Table 1, where the plasma density model is taken from *Streltsov and Lotko* [2003], while the temperature ratio τ is assumed to be 10. The electron inertia length λ_e is larger than the ion Larmor radius ρ_i in the range of $s \approx 1$–3 R_E; around $s \approx 4$ R_E, these two are the same order [*Stasiewicz et al.*, 2000]. B_0 and L_c are calculated with the Tsyganenko-96 model, e.g., L_c = 7 R_E, used as a typical curvature radius at the substorm recovery phase. The observation site in *Shiokawa et al.* [2010] is located at a flux tube of $L \approx 6.9$, for which the field-line position at equator is calculated to be $s_{eq} \approx 7.5$ R_E. Here we assume the scale of a standing wave to be $L_\parallel = s_{eq}/2$ throughout the field line. The perpendicular scale $L_\perp$, standing for the flux tube, is also determined to resolve the electron inertia length, e.g., $L_\perp \approx 407$ km at $s = 4$ R_E.

[12] For spatial derivatives, we use the spectral method with a dealiasing filter over the wave number $k = N/3$, where N = 512 is the number of meshes in both x and y directions. Here we assign the periodic boundary condition in both directions. Although we made an another calculation using fourth-order center differencing method, the spectral method is so appropriate for resolving high current shears and electron inertia effects. For time integration, we used fourth-order Runge-Kutta-Gill method, and the time resolution is variable in accord with the Courant-Friedrichs-Lewy condition as $v_{max}\Delta t/\Delta x < 0.3$; $v_{max} = (b_0 \times \nabla_\perp \phi)_{max}$ is the maximum electric drift velocity in the domain, and the right-hand number is set to be sufficiently small. We provide as the initial condition a small perturbation in p with a magnitude of 10^{-10} (normalized) and a white-noise type distribution with a random number. We try to demonstrate a fingerlike structure to be formed even when it starts from a purely unperturbed condition. Other variables ϕ and ψ are set to be zero, which means no flow and field-aligned current initially.

3. Results

[13] We present our simulation results at field-line positions of s = 4 R_E and 7.5 R_E; the latter corresponds to the plasma sheet where the ion beta is set to be unity. Figure 1 shows a cross-sectional distribution at s = 4 R_E of the field-aligned current $j_\parallel$ in unit of μA/m^2 at times of (a) t = 67.4 s and (b) 71.4 s; model parameters are $\alpha = 1.70 \times 10^{-2}$, $\beta' = 1.13 \times 10^{-6}$, $\kappa = 9.11 \times 10^{-3}$, $\delta = 0.214$, and $\delta_e = 1.00 \times 10^{-4}$. The physical unit is obtained from a calculated value being multiplied by $j_{\parallel s} = B_0/\mu_0 L_\perp$ in SI units. Figure 1c shows time variations in the normalized energies of electric ($\frac{1}{2}|\nabla\phi|^2$), magnetic ($\frac{1}{2}|\nabla\psi|^2$), and pressure fields ($\frac{1}{4}(1+\tau)p^2/\beta$) averaged in space [*Hazeltine et al.*, 1987]. The energy of the pressure field is much smaller than the other two energies, in which the difference is larger than the highest order ($\approx 10^2$) of the spatial derivative or $k_\perp$. Note that the wave number k is divided by $2\pi/L_\perp$ rad/km) with the system size $L_\perp$ in our definition. However, the linear growth behavior in all energies is realized up to $t \approx 70$ s. In the linear growth phase as in Figure 1a, small-scale patches characterized by wave numbers $k_y \approx 3$–4 (or wavelengths λ_y = 80–120 km) are produced. After the time of $t \approx 70$ s, energies approach a stationary point owing to the nonlinear effect, and the small-scale patches fragment into fingerlike structures aligned in y direction with a scale of 20–50 km; they appear throughout the system, e.g., [x, y] = [100, 180] and [280, 300] in Figure 1b. The dual-scale behavior is consistent with the formation of fingerlike structures in the patch auroras [*Shiokawa et al.*, 2010]. It should be mentioned that the number of fingers varies from site to site, both in our calculation and in their observation. The value of $j_\parallel$ becomes up to 4 μA/m^2. We suppose that structures in the field-aligned current at this height correspond to the auroral luminosity at the ionospheric height ($\approx$100 km) because nonthermal electron acceleration is assumed not to occur in the patch aurora area.

[14] The ion inertia length λ_i being 174 km at s = 4 R_E as described in Table 1, the scale of patches (80–120 km) is slightly less than $0.7\lambda_i$; the system size (407 km) is $2.42\lambda_i$. We identify these structures driven by the ion diamagnetic drift wave by comparing them with a previous study of the Rayleigh-Taylor instability [*Huba et al.*, 1998]. The linear growth rate is shown as a function of mode number k_y in Figure 2 of their paper, and it has a maximum around k_y = 16 including the FLR effects. As the system size is $11.9\lambda_i$ in their case, the scale of the k_y = 16 mode is $0.74\lambda_i$ and is almost equal to that of the patches obtained here. We confirmed that higher modes are quickly damped in the initial phase as indicated by their linear analysis. It is also pointed out that the isotropy, or existence of k_x modes, is originated from

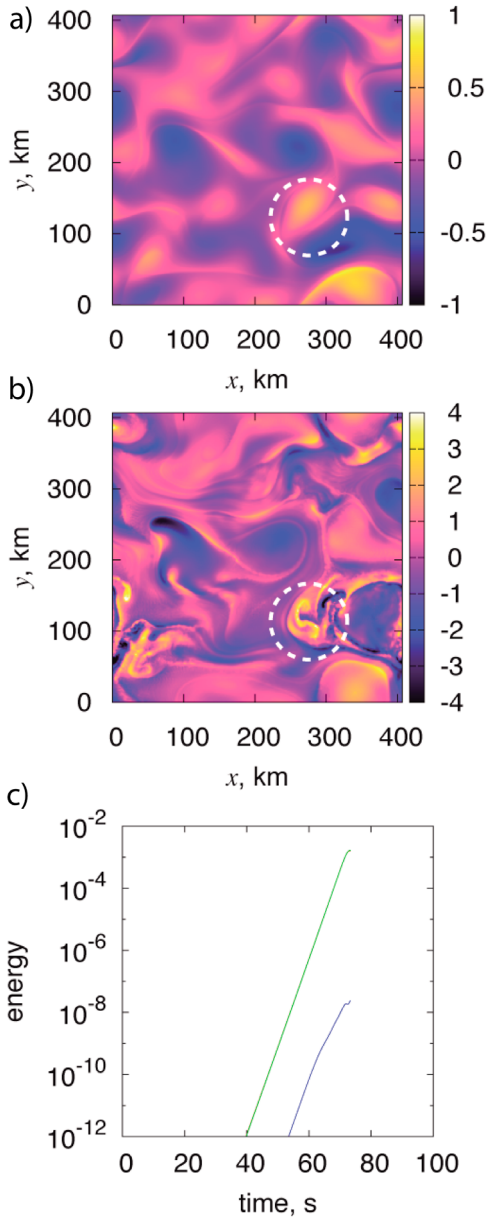

Figure 1. Cross-sectional distribution of the field-aligned current $j_{\|}$ in unit of μA/m^2 at times of (a) t = 67.4 s (linear growth phase) and (b) 71.4 s (saturation phase). Control parameters are provided by assuming the condition of a field-line position s = 4 R_E. Fragmentation of small-scale patches is clearly seen around, e.g., [x, y] = [100, 180] and [280, 300] in Figure 1b. Note that the system size is scaled as ≈38 km by the ionospheric mapping, fingerlike structures to be ≤5 km. A dashed circle shows the area mapped into a radius of 5 km at the ionosphere. (c) Time variations in normalized energies of electric (red), magnetic (green), and pressure fields (blue); the red line is overlapped by the green line.

the low-β condition; if β and p are large, k_y modes dominate in the linear phase owing to the interchange effects in equations (1) and (3).

[15] On the other hand, fingerlike structures in fragmentation of patches are driven by the electron inertia effect or the final term in equation (2). As the field-aligned current $j_{\|}$ increases rapidly, the nonlinear cascade occurs down to scales of 5–12λ_e ($k_x \approx$ 8–12), where the electron inertia length λ_e = 4.07 km. The associated magnetic fluctuations can be continuously supported by the ion drift wave along with the magnetic curvature. We solve directly the electron inertia term with a small time resolution and thus cannot analyze the longtime behavior of fingerlike structures in detail; it is the reason for the closeness of snapshots in Figures 1a and 1b, but a dramatic change in patch structures appears in the nonlinear phase. The scale (≈1 minute) of the modeled finger development fairly agrees with the minimum scale

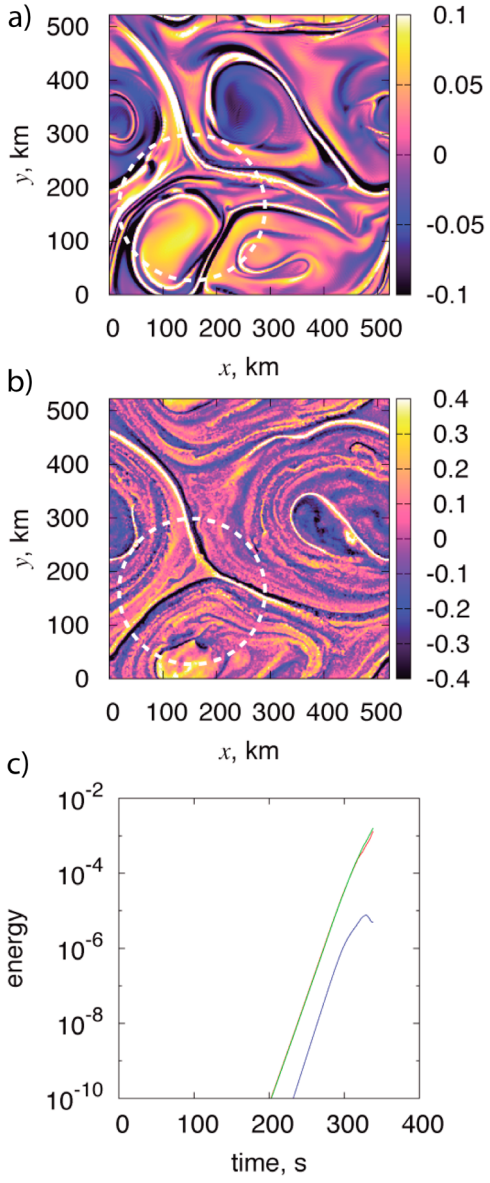

Figure 2. Same as Figure 1 but at times (a) t = 314 s (linear growth phase) and (b) t = 330 s (saturation phase), and the condition of control parameters is assumed on the plasma sheet (s = 7.5 R_E, β_i = 1). In this case, no fingerlike structures appear; instead, large-scale convections dominate. Note that the system size is scaled as ≈19 km by the ionospheric mapping. (c) Time variation in normalized energies; a red line overlaps a green line.

(2 minutes) reported in *Shiokawa et al.* [2010], considering uncertainties in the model parameters. Besides the spatial scale mentioned above, it should be pointed on the direction of the fingerlike structures. These structures typically develop in the east–westward direction, or having a wave number k_x in our definition, and our result indicates a similar tendency. This anisotropic behavior is originated from the nature of the drift wave, i.e., modes with a variety of k_y but $k_x \approx 0$ are likely to be unstable. Although the mode distribution seems to be isotropic in the plot of $j_\parallel$ in Figure 1, the vector potential ψ as well as ϕ and p (not shown) has a strong anisotropic behavior, i.e., $k_y = 1$ and $k_x \approx 0$, from the very initial growth phase; its positive peak is positioned around the center $y = L_\perp/2$. As the current $j_\parallel$ increases, higher k_x modes in ψ, hence $j_\parallel$, are produced owing to the nonlinear coupling between modes with $\partial_x j_\parallel$ and the $k_y = 1$ mode with $\partial_y \phi$ in the Poisson bracket $\{\phi, j_\parallel\}$ in equation (2). Thus, the fingerlike structures ($k_x \approx 8$–12) are formed at the east/west vicinities of patches as seen in the above observations. In other words, the fingers appear when the lowest-mode drift wave ($k_y = 1$) begins to convert energies to other finite k_x modes.

[16] We can compare the spatial scale by ionospheric mapping with an assumed local flux tube magnetic field geometry (Tsyganenko model). From an image of their observation, the patch scale is estimated to be 10–20 km, while the fingerlike structure is to be ≤5 km. The relation $B_0 h_\nu h_\varphi = \text{const}$ holds in a flux tube, where h_ν and h_φ are the scaling factors in the latitudinal and longitudinal directions, respectively; $h_\nu = h_\varphi = 1$ at the ionosphere. Considering the flux tube of $L = 6.9$ in their observation site and the ratio of $B_0(4\ R_E)/B_0(100\ \text{km})$, we estimate an averaged characteristic (system) scale $L_\perp \approx 38$ km at the ionosphere where $\sqrt{h_\nu h_\varphi} \approx 10.7$ is used. In the same way, the patch scale is 7.4–11 km, while the fingerlike structure is scaled to be 1.9–4.7 km, both of which are consistent with those obtained from observation. Slight differences may be originated from uncertainties in some plasma parameters as density and magnetic field, controlling δ_e and $h_\nu h_\varphi$ (see also section 4).

[17] We reproduced essentially the same fingerlike structure along with underlying processes from calculations at field-line positions of $s = 2\ R_E$ and $6\ R_E$, except for the spatial and temporal scales. The difference in the spatial scale is originated from those in ion and electron inertia lengths as shown in Table 1. However, scales of the fingerlike structure by ionospheric mapping are estimated to be a few kilometers in any case. The time scale varies from ≈ 25 s at $s = 2\ R_E$ to ≈ 170 s at $s = 6\ R_E$, which is mainly determined by the local Alfvén velocity; it slightly depends on the magnetic curvature, increasing with field line position by a factor of 2. The relative amplitude of the field-aligned current also has an order of difference; ≈ 10 μA/m^2 at $s = 2\ R_E$ and ≈ 1 μA/m^2 at $s = 6\ R_E$. Contribution of each height to the auroral luminosity is discussed again in the next section.

[18] Finally, we examine the behavior of the field-aligned current at the plasma sheet, $s = 7.5\ R_E$. The point is whether the dual-scale (patch and fingerlike) structures identified in low-β regimes are really produced in the high-β environment. Figure 2 shows cross-sectional distributions of the field-aligned current $j_\parallel$ in unit of μA/m^2 at times of (a) $t = 307$ s and (b) 330 s, along with (c) time variations in averaged field energies; model parameters are $\alpha = 2.18 \times 10^{-2}$, $\beta' = 1.16 \times 10^{-3}$, $\kappa = 1.16 \times 10^{-2}$, $\delta = 0.214$, and $\delta_e = 1.00 \times 10^{-4}$. The pressure field energy (e.g., $t = 330$ s) is > 2 orders of magnitude higher than that of the case in Figure 1c (e.g., $t = 70$ s), which corresponds to a first- to second-order difference in the pressure, or beta. The electron temperature ($T_e/e \sim \langle \delta p \rangle \approx 10^{-3}$) is slightly smaller than the electric and magnetic potentials ($\langle \phi \rangle \approx 10^{-2}$); thus the ion temperature $\langle \delta \tau p \rangle$ is comparable with these potentials. As seen in the above case, ion diamagnetic drift modes grow up in the initial phase, though the wave number distribution is anisotropic as $k_y \approx 4$ and $k_x \leq 1$. Different from the case of $s = 4\ R_E$, large-scale convective flows are produced at the middle stage of linear growth $t = 100$–300 s by some pressure-driven instability related to the right-hand term in equation (3). In Figure 2a, the wavelength of the vortex structure is about $2\lambda_i$; here the ion inertia length $\lambda_i \approx 224$ km. Modes with smaller scales are considered to be collapsed or damped through a dynamic motion of the large-scale vortices. After the pressure field saturates around $t \approx 330$ s, an inverse cascade to the $k_x = k_y = 1$ mode occurs and it dominates in the system; several fine structures appear with the lowest mode being an envelope. Note that the system size, or the scale of $k_y = 1$, is estimated to be ≈ 19 km by ionospheric mapping. However, any fingerlike pattern is not observed in the subsequent dynamics of $j_\parallel$ within the time scale of 1–6 minutes, i.e., the scale of fingerlike structures obtained from observations. It is also pointed that the maximum value of $j_\parallel \approx 0.4$ μA/m^2 is much smaller than that in the case of $s = 4\ R_E$.

4. Discussion

[19] We examine the wave numbers of patch and fingerlike structures obtained for the case of $s = 4\ R_E$ in Figure 1 with a two-dimensional fast Fourier transform analysis. The mode power spectra $P = |\tilde{j}_\parallel|^2$ of two plots in Figures 1a and 1b are shown as a function of wave numbers k_x and k_y in Figure 3; normalized values are used. Note that the distribution of $P(k_x)$ is provided by a spatial average in the y direction, while $P(k_y)$ is averaged in the x direction. We find that a clear power law spectrum well fit by a function $\sim k_{x,y}^{-2.6}$ is realized in the linear growth phase for the wave number range between ion ($k_x = 2.3$) and electron ($k_x = 100$) inertia lengths. Remarkable shifts from the spectrum are formed at $k_x = 3$–5 and $k_y = 3$–7 that are considered to be responsible for small-scale patches in Figure 1a. The spectrum is almost isotropic, as mentioned in section 3, within a factor of difference between $P(k_x)$ and $P(k_y)$. There are some shifts or peaks in the range of $k_y = 8$–16 that might be an indication of generation of fingerlike structures. In the nonlinear phase (Figure 1b), the power spectrum becomes large owing to an energy input by the drift instability and is fit by a harder spectrum of $\sim k_{x,y}^{-1.8}$, being almost identical to a Kolmogorov type. It can be speculated that the ion velocity has a similar spectrum due to the convective term $\{F, \zeta\}$, and the effect is converted to the current one through the interaction between electric and magnetic energies. On the other hand, the increasing rate of the power spectrum of lower modes $k_{x,y} = 2$–6 is relatively small, indicating an energy cascade to higher modes due to the patch fragmentation. We clearly identify the dual-scale (patch and finger) structures from the peaks attained in $P(k_x)$, i.e., $k_x = 4$–7 to a patch and $k_x = 8$–11 to a finger. The spectrum in $P(k_y)$ is somewhat featureless, although it reveals a weak antiphase oscillation to $P(k_x)$.

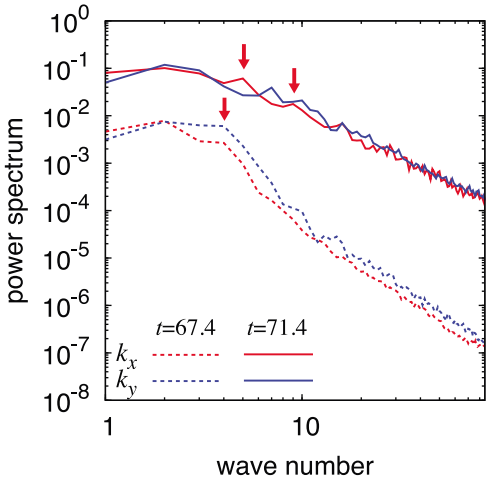

Figure 3. Power spectra P of $j_\parallel$ as a function of wave numbers k_x (red) and k_y (blue) at two periods in the case of a field-line position $s = 4\ R_E$. Lower two lines show the spectra obtained from a plot in Figure 1a ($t = 67.4$ s) and higher two show those in Figure 1b ($t = 71.4$ s). Note that $P(k_x)$ is provided by an average in the y direction, while $P(k_y)$ is averaged in the x direction. Dual scale structures (patches and fingers) appearing in Figure 1 are well identified from the peaks in $P(k_x)$ distribution at the nonlinear period; $k_x = 4$–7 to a patch and $k_x = 8$–11 to a finger with arrows.

[20] We studied the β dependence on auroral (field-aligned current) structures in the previous section. Here we briefly mention the effects of other model parameters such as the temperature ratio τ and the magnetic curvature κ. We assumed $\tau = T_i/T_e = 10$, as the electrons are typically cold in the plasma sheet area. However, that is not necessarily satisfied along a field line where a variety of wave-particle interactions occurs, and it is useful to examine the effect of high T_e. Setting $\tau = 1$ with increasing T_e, we make a similar calculation as in Figure 1 and obtain the temporal behavior of field-aligned current $j_\parallel$; other parameters and model conditions are identical. In this case, the fingerlike structures are reproduced at some points of the system at time $t \approx 72$ s (not shown). The pressure field energy reaches a stationary point in this phase, and 1–2 seconds later other energies indicate a similar tendency. These behaviors are identical to the case in Figure 1, except for the magnitude, one order of increase for pressure and tens of percentage decrease for others. We conclude that if β is constrained to be $\ll 1$ (as 10^{-2}), the fingerlike structures can be produced in a wide range of τ.

[21] The field-line scale of a standing wave α ($= L_\parallel/L_\perp$) changes slightly the linear growth rate. The time scale becomes smaller if a larger $k_\parallel$ mode exists, whereas it increases only tens of percent even if $L_\parallel$ becomes as large as 7.5 R_E. A factor of difference in the time scales between our result (≈70 s) and Shiokawa's (≥2 min) is not explained within the limitation of 2.5-dimensional model. Effects of the term $\nabla_\parallel j_\parallel$ on the growth time as well as Alfvén wave dynamics should be analyzed elaborately with a three-dimensional simulation. The magnetic curvature κ changes the saturation level of all energies, resulting in a higher field-aligned current or auroral luminosity. Estimation of the actual curvature radius from observations is desired to reduce the uncertainty in κ, since we only employ the flux tube model to give $L_c \approx 7\ R_E$. Finally, δ and δ_e are associated with the ion and electron inertia lengths $\lambda_{i,e}$ and can change the scales of patch and fingerlike structures. To reduce this uncertainty, we stimulate future observations of plasma density along with its response to some external energy inputs at a substorm period. It is, however, noted that the relative scales of patch and finger are unchanged, since the ratio $\delta/\delta_e \sim \lambda_i/\lambda_e$ is identical for any plasma density.

[22] We presented formation of fingerlike structures in a low-β regime (2–6 R_E) in the previous section, but the time scale of their appearance varies as largely as 25–170 s. The lower value is realized by a high Alfvén velocity up to 10^9 cm/s or by a sharp density drop near $s = 2\ R_E$, against a strong magnetic field. The large time variation cannot be reduced at any condition, since the plasma density is unlikely to vary over one order of magnitude. It is thus natural to consider that structures formed in a short time scale coexist with those formed in a long time scale in appearance at the ionosphere. The time scale >2 min is favorable in the condition for the observations by *Shiokawa et al.* [2010], which means that in our criterion, structures at the regime of $s > 5\ R_E$ survive, while shorter-scale structures are fully cut off for some reason. We have not proposed a good reason for this selection without a full three-dimensional analysis of parallel mode dynamics as mentioned at the discussion of α. As for the magnitude of the field-aligned current, there is no particular region to be selected, because it becomes higher with decreasing field-line position s. The curvature radius typically seems to have a minimum around $s = 4$–6 R_E, but a further restriction would be done by providing its actual field-line distribution as pointed out just above.

[23] The necessity of further studies is also inferred from the observational fact. It is found from the image data in *Shiokawa et al.* [2010] that fingerlike structures are collapsed by a large-scale convection after they grow up to a certain extent. Here we emphasize that the growth time scale of fingers is coincidentally on the same order as the Alfvén transit time on a field line, $t_A \sim L_\parallel/v_A \approx$ a few minutes. The Alfvén wave can be excited simultaneously with the appearance of the perpendicular structures, carrying information along a field line. As a result, fingers produced in patch fragmentation may be stabilized through a transport of large-scale flow patterns from the plasma sheet by the Alfvén wave. The coupling process between these fine structures and the parallel modes, related to the lifetime of fingers, along with auroral pulsation should be studied. However, we consider that the essence of the finger formation is independent of the parallel mode dynamics and is well reproduced by our 2.5-dimensional simulation. The assumption that all field variables are quasi-constant within a scale of $L_\parallel = s_{eq}/2$ (3.75 R_E) in deriving equations (1)–(3), e.g., $\langle \nabla j_\parallel \rangle = \int \nabla j_\parallel ds L_\perp/L_\parallel = \alpha j_\parallel$, is validated from our simulation results; identical structures were obtained in the low-β regimes, although the time scale of their dynamics should be resolved by further detailed studies.

[24] We briefly mention the mechanism of a different type of small-scale structures observed by Reimei satellite [*Ebihara et al.*, 2010]. We present a simple story from our calculations that the drift wave is first excited in the region of high electron pressure gradient β', and patchy structures in the field-aligned current are formed along the field line. Then the

electron inertia effect produces smaller (finger) structures due to an increase in the field-aligned current in the off high-β regions. Wavy or smokelike shapes seen in patch auroras combining k_x and k_y modes imply that their driver β' points forcibly to a multiple direction due to an intense hot electron flow. This high β' process need not have any assumption on the condition of cold plasmas. However, other possibilities can be considered by a particle scattering by whistler waves or a cold plasma turbulence. The lower-hybrid mode with scales $\leq \lambda_i$ can be captured when the Hall effects are fully treated; it seems that these high k modes may not be unstable, when the inertia length λ_i is comparable to the Larmor radius ρ_i, due to the FLR effect. We suppose that the lower-hybrid mode is responsible for the finger structure if it is still unstable or ρ_i is still $\ll \lambda_i$; otherwise, the electron inertia effect in low-β regime has a major contribution if the gradient β' is essential. We may restrict possible mechanisms for smoky and finger structures by studying the auroral response to the electron and ion pressure enhancements. Anyway, it can be said that various shapes of diffuse auroras would appear, besides the two types discussed in this paper, through the response of inner magnetospheric field lines.

5. Conclusions

[25] We reproduce a dual-scale auroral structure (patch and finger) appearing in recent observations by a reduced MHD model simulation with the ion and electron inertia effects at a low-β plasma condition of $s = 2$–$6\ R_E$; on the other hand, the finger cannot appear and a large-scale vortex flow pattern dominates in the system of the plasma sheet ($s = 7.5\ R_E$). The scales of patches and fingers produced at $s = 4\ R_E$ are estimated to be 7.4–11 km and 1.9–4.7 km, respectively, by ionospheric mapping. It is also found that patches reveal an isotropic mode structure, and fingers with an anisotropic k_x mode develop in the east–west direction. We present the mechanism that (1) an ion diamagnetic drift mode grows uniformly along a field line, including the plasma sheet, in accord with a magnetic energy input, and (2) a secondary fingerlike structure due to the electron inertia effect is excited in a low-β regime out of the plasma sheet and makes patch auroras fragmented. Our future studies should clarify a factor of difference in the time scale of finger formation between our result (≈70 s) and observation (>2 min) along with the effects of the parallel mode dynamics.

[26] **Acknowledgments.** We thank Kazuo Shiokawa for useful discussions with his auroral data.

[27] Robert Lysak thanks Vincent Genot and another reviewer for their assistance in evaluating this paper.

References

Akasofu, S.-I. (1974), A study of auroral displays photographed from the DMSP-2 satellite and from the Alaska meridian of stations, *Space Sci. Rev.*, *16*, 617–725.

Aydemir, A. Y. (1992), Nonlinear studies of $m = 1$ modes in high-temperature plasmas, *Phys. Fluids B*, *4*(11), 3469–3472.

Braginskii, S. I. (1965), *Review of Plasma Physics*, vol. 1, ed. M. A. Leontovich, Consultants Bureau, New York.

Chaston, C. C., V. Genot, J. W. Bonnell, C. W. Carlson, J. P. McFadden, R. E. Ergun, R. J. Strangeway, E. J. Lund, and K. J. Hwang (2006), Ionospheric erosion by Alfvén waves, *J. Geophys. Res.*, *111*, A03206, doi:10.1029/2005JA011367.

Chaston, C. C., C. Salem, J. W. Bonnell, C. W. Carlson, R. E. Ergun, R. J. Strangeway, and J. P. McFadden (2008), The turbulent Alfvéic aurora, *Phys. Rev. Lett.*, *100*(17), 175003.

Davis, T. N. (1978), Observed characteristics of auroral forms, *Space Sci. Rev.*, *22*, 77–113.

Ebihara, Y., T. Sakanoi, K. Asamura, M. Hirahara, and M. F. Thomsen (2010), Reimei observation of highly structured auroras caused by non-accelerated electrons, 115, A08320, doi:10.1029/2009JA015009.

Goldstein, J., J. L. Burch, B. R. Sandel, S. B. Mende, P. C:son Brandt, and M. R. Hairston (2005), Coupled response of the inner magnetosphere and ionosphere on 17 April 2002, *J. Geophys. Res.*, *110*, A03205, doi:10.1029/2004JA010712.

Hazeltine, R. D., C. T. Hsu, and P. J. Morrison (1987), Hamiltonian four-field model for nonlinear tokamak dynamics, *Phys. Fluids*, *30*, 3204–3211.

Huba, J. D., and D. Winske (1998), Rayleigh-Taylor instability: Comparison of hybrid and nonideal magnetohydrodynamic simulations, *Phys. Plasmas*, *5*, 2305–2316.

Lewis, W. S., J. L. Burch, J. Goldstein, W. Horton, J. C. Perez, H. U. Frey, and P. C. Anderson (2005), Duskside auroral undulations observed by IMAGE and their possible association with large-scale structures on the inner edge of the electron plasma sheet, *Geophys. Res. Lett.*, *32*, L24103, doi:10.1029/2005GL024390.

Lui, A. T. Y., C.-I. Meng, and S. Ismail (1982), Large amplitude undulations on the equatorial boundary of the diffuse aurora, *J. Geophys. Res.*, *87*, 2385, doi:10.1029/JA087iA04p02385.

Lysak, R. L., and Y. Song (2008), Propagation of kinetic Alfvén waves in the ionospheric Alfvén resonator in the presence of density cavities, *Geophys. Res. Lett.*, *35*, L20101, doi:10.1029/2008GL035728.

Nishitani, N., G. Hough, and M. W. J. Scourfield (1994), Spatial and temporal characteristics of giant undulations, *Geophys. Res. Lett.*, *21*(24), 2673–2676, doi:10.1029/94GL02240.

Rankin, R., J. C. Samson, V. T. Tikhonchuk, and I. Voronkov (1999), Auroral density fluctuations on dispersive field line resonances, *J. Geophys. Res.*, *104*, 4399–4410, doi:10.1029/1998JA900106.

Shiokawa, K., A. Nakajima, A. Ieda, K. Sakaguchi, R. Nomura, T. Aslaksen, M. Greffen, and E. Donovan (2010), Rayleigh-Taylor type instability in auroral patches, *J. Geophys. Res.*, *115*, A02211, doi:10.1029/2009JA014273.

Stasiewicz, K., P. Bellan, C. Chaston, C. Kletzing, R. Lysak, J. Maggs, O. Pokhotelov, C. Seyler, P. Shukla, L. Stenflo, A. Streltsov, and J-E. Wahlund. (2000), Small scale Alfvénic structure in the aurora, *Space Sci. Rev.*, *92*, 423–533.

Streltsov, A. V., and W. Lotko (2003), Reflection and absorption of Alfvénic power in the low-altitude magnetosphere, *J. Geophys. Res.*, *108*(A4), 8016, doi:10.1029/2002JA009425.

Yamamoto, T., K. Makita, and C.-I. Meng (1993), A particle simulation of giant undulations on the evening diffuse auroral boundary, *J. Geophys. Res.*, *98*(A8), 5785–5800, doi:10.1029/93JA00641.

Zhang, Y., L. J. Paxton, D. Morrison, A. T. Y. Lui, H. Kil, B. Wolven, C.-I. Meng, and A. B. Christensen (2005), Undulations on the equatorward edge of the diffuse proton aurora: TIMED/GUVI observations, *J. Geophys. Res.*, *110*, A08211, doi:10.1029/2004JA010668.

Y. Hiraki, National Institute for Fusion Science, Oroshi-cho 322-6, Toki, Gifu, 509-5292, Japan. (hiraki.yasutaka@nifs.ac.jp)

K. Sakaguchi, National Institute of Information and Communications Technology, Nukui-kita 4-2-1, Koganei, Tokyo, 184-8795, Japan.